Projekt záró beszámoló

We have published four papers in Q1 ranked journals from the results of the project so far (Mikó-Baráth et al., 2014; Kóbor et al., 2017; Budai et al., 2018; Horváth et al., 2018a). Another manuscript has been submitted (Telkes et al., 2018) and two others are in preparation (Horváth et al., 2018b; Radó et al., 2018). In the following, we briefly summarise the main results of these studies in a logical rather than chronological order.

Three dimensional display technology is widely used in vision research as well as in medicine, space research and entertainment. In order to create the illusion of a three dimensional visual scene on flat displays, dichoptic stimulation is needed, that is, the two eyes have to be presented with slightly different but clearly separated images. The most perfect image separation can be provided by the stereoscope but it requires two displays and a finely adjustable optical system to allow fusion of the two images. Fusion is still difficult for some viewers (children for instance) due to the unnatural viewing situation. Techniques utilizing shutters to present the two images in an alternating fashion are prone to cross-talk as well as flicker.

The most economical and thus, wide-spread solution to these problems is to present the two images simultaneously and to separate them based on their spectral composition or light polarization using colored or polarizing filter goggles, respectively. The channel separation is however, never perfect due to imperfection of physical filters resulting in more or less cross-talk. When viewing a conventional stereogram such as in 3D cinema, uncompensated filter cross-talk results in image ghosts where each eye also receives the shifted image intended for the other eye. A certain amount of cross-talk can be neglected in entertainment applications but in vision research, it can severely bias scientific results and conclusions.

Stereopsis is also sensitive to interocular differences in luminance as well as contrast. A well-known example of the effect of interocular luminance difference is the Pulfrich-effect, which is due to luminance dependent differences in processing time in the visual pathways (Markó et al., 2012). The same effect can deteriorate the depth percept in stereo kinematograms. Interocular contrast differences on the other hand, rapidly deteriorate binocular fusion, whereas equalizing interocular contrast restores it. This phenomenon is often referred to as contrast paradox in stereopsis.

Besides eliminating ghosting and equalizing interocular luminance and contrast, it is often desirable that the average luminance and contrast of stereoscopic displays be precisely controlled. Finally, physical limitations of the specific displays and filters used will limit the extent to which this complex set of requirements can be fulfilled.

Dynamic random dot stereograms (DRDSs) and correlograms (DRDCs) are visual stimuli originally invented by Béla Julesz (Julesz, 1960) in order to selectively activate low-level disparity sensitive mechanisms of the visual system. A strict requirement for the utility of DRDSs is that the three-dimensional (3D) pattern be only visible by binocular viewing and functional stereoscopic vision whereas monocular viewing or dysfunctional stereopsis would result in a meaningless random dot pattern for either eye. Monocular cues (also called monocular artefacts in the current context) on the other hand, can result in responses from monocular perceptual mechanisms essentially based on luminance contrast. In such cases, the responses, whether behavioral or neurophysiological, could be confounded with responses of the stereoscopic mechanism.

In a manuscript currently in preparation (Radó et al., 2018), we demonstrate the concept of properly calibrating a stereoscopic display on the simple example of an anaglyphic random dot correlogram.

As we will show, DRDCs provide an especially useful testing ground for proper calibration because failures of eliminating monocular artefacts result in easily detectable monocular cues (Fig. 1).

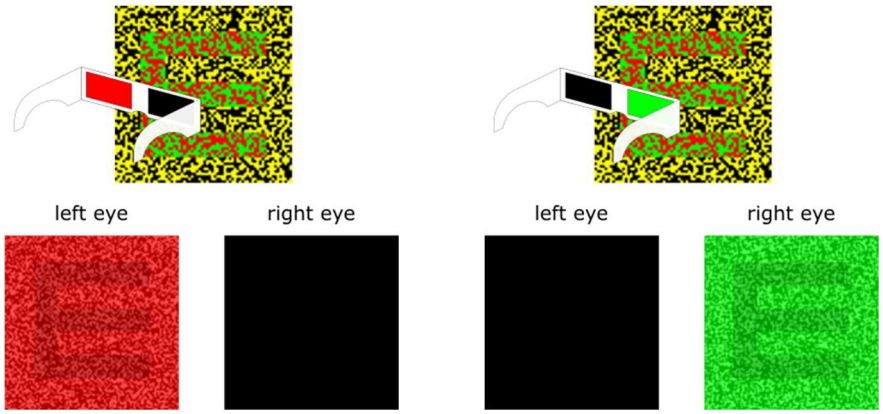

Figure 1**. Schematic representation of the monocular views of the anaglyphic DRDC frame shown in** Error! Reference source not found. **if the anaglyphic colors are 'spoiled', i.e. deviate from optimal calibration. Images at the top of each panel show the same stimulus frame. Panel A illustrates that in this case, the Snellen-E target becomes visible if the stimulus is viewed monocularly through the left (red) filter of a red-green goggle. Note that the exact appearance of the background and target regions can be different depending on which of the colors deviate from the optimum and in which direction. Panel B shows the same for viewing through the right (green) filter.**

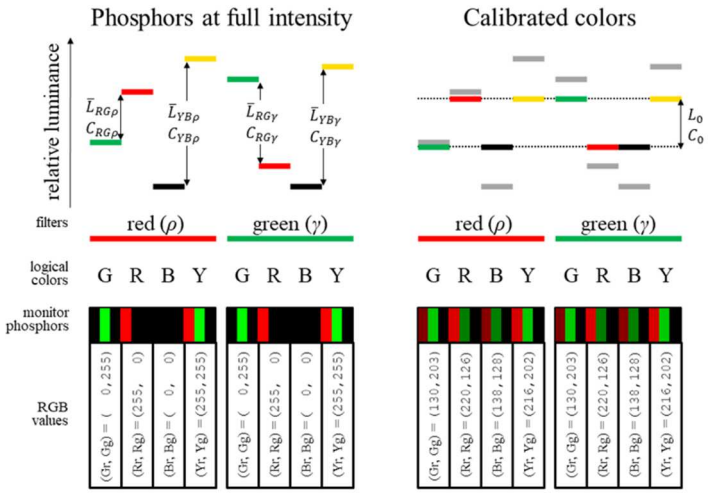

Figure 2**. Schematic demonstration of the problem and its solution.**

Our aim was to selectively stimulate the stereoscopic visual mechanism using cyclopean random dot patterns that perceptually consist of bright and dark dots. These stimuli are ideally free from monocularly detectable cues. In order to eliminate monocular cues, bright dots must have perceptually equal luminances irrespective of the logical color (G, R, B, Y in Fig. 2) or the color filter (red or green in Fig. 2). The same must apply for the dark dots. We specify the required values by the average luminance (L_0) and contrast (C_0).

Our task was to find the red (**r**) and green (**g**) phosphor values (8 RGB values shown in the bottom row of the Fig. 2) of each of the logical colors so that the above requirements are met. The inputs of the algorithm were L_0, C_0 and the measured luminance characteristics of the **r** and **g** phosphors through each of the color filters.

We obtained the solution by numerical optimization using least-square minimization of the following error terms for luminance and contrast, respectively:

$$||\boldsymbol{e}_L|| = \frac{1}{L_0^2}\left\|\left[\left(L_0 - \overline{L}_{RG\rho}\right)^2, \left(L_0 - \overline{L}_{RG\gamma}\right)^2, \left(L_0 - \overline{L}_{YB\rho}\right)^2, \left(L_0 - \overline{L}_{YB\gamma}\right)^2\right]\right\|$$

$$||\mathrm{e_C}|| = \frac{1}{\mathrm{C_0^2}}\left\|\left[\left(\mathrm{C_0 - C_{RG\rho}}\right)^2, \left(\mathrm{C_0 - C_{RG\gamma}}\right)^2, \left(\mathrm{C_0 - C_{YB\rho}}\right)^2, \left(\mathrm{C_0 - C_{YB\gamma}}\right)^2\right]\right\|$$

Here, $\overline{L}_{RG\rho}$ is the average luminance and $C_{RG\rho}$ is the Michelson-contrast of the *R* and *G* colors perceived through the *red* filter etc. as shown in Fig. 2. It was also possible to find an analytical solution to zeroing the error terms using the Mathematica package.

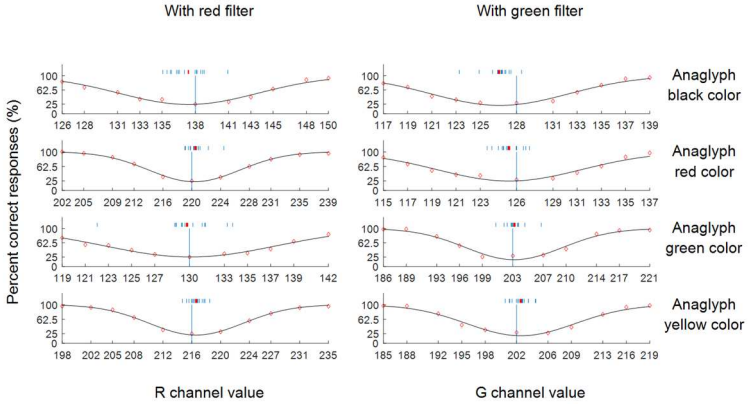

Figure 3. **Determining the empirical optima of R and G values for each of the anaglyphic colors. Red diamonds indicate the average of percent correct responses of 16 participants. Vertical blue line indicates the value predicted by our model. Black lines show inverted Gaussian curves fitted to these average values and their minima are indicated by the red tick marks. Similar Gaussians were fitted to the responses of each participant and their minima are indicated by blue tick marks.**

We demonstrated in psychophysical tests that the stimulus calibrated by this procedure is free from monocular cues (Fig. 3). The largest deviation of the median empirical optimum from the prediction was -1.25 RGB units (upper right data set in Fig. 3) indicating that the optima calculated by our procedure correspond to perceptually defined optima within the luminance resolution of the display. We also implemented this method for displays using channel separation by polarizing filter goggles. This opened the way for designing binocular visual stimuli for experiments probing stereoscopic mechanisms.

In much of the current project, we were interested in the temporal aspects of neural processing in the stereoscopic or colour vision systems. In the study of Mikó-Baráth et al. (2014), we studied latency changes in the visual evoked potential to cyclopean DRDC stimuli during maturation of preterm and full-term infants. The P1 wave is the major positive component of pattern-reversal visual evoked potentials (PRVEPs). The rapid decrease of its latency correlates with the progressive myelination in the developing infant brain, which affects signal transmission in the visual system. An age dependent phase shift, analogous to P1 peak latency, can also be observed in dynamic random

dot correlogram (DRDC)-evoked steady state VEPs (DRDC-VEPs), an objective method used to assess binocular function. The objectives of this study were (1) examination of DRDC-VEP phases in preterm and full-term infants as a function of age after the onset age of binocularity; (2) to determine whether DRDC-VEP phases depend on visual experience or are an experience-independent developmental process; and (3) to study the relationship between DRDC-VEP phases and PR-VEP P1 peak latencies. DRDC-VEPs and PR-VEPs were recorded in 128 full-term and 47 preterm healthy infants and toddlers. DRDC stimuli were presented on the red and green channels of a CRT monitor while infants wore red-green goggles for dichoptic viewing. Reliability of VEP responses was assessed by the T^2_{circ} statistic (Victor and Mast, 1991). Logistic function was fit to the phase and latency data as a function of age, and goodness of fit was assessed by analysis of residuals.

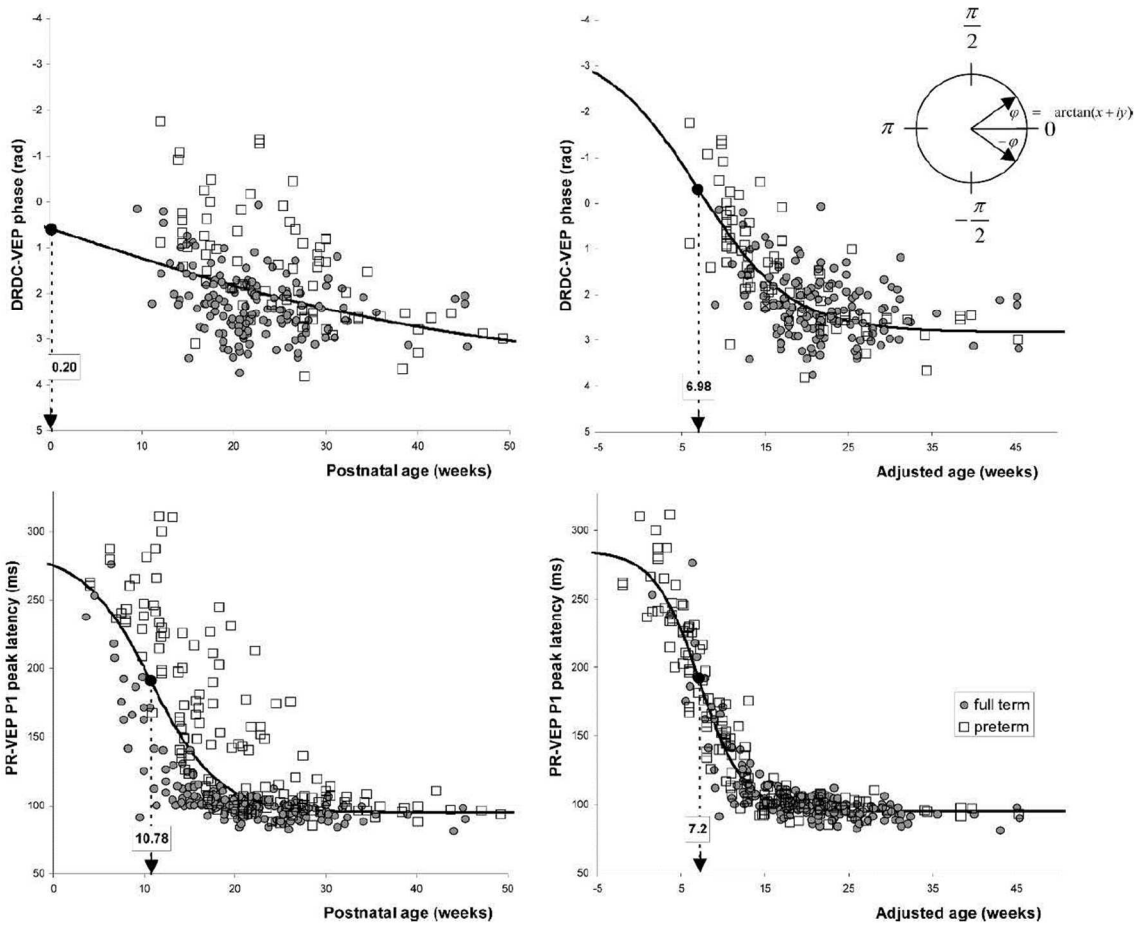

Figure 4. **Top: The relationship between age and DRDC-VEP phases. DRDC-VEP phases of the second harmonic Fourier components (i.e., 3.75 Hz) of the DRDC fundamental frequency (i.e., 1.875 Hz) are plotted in rads as a function of adjusted and postnatal ages in weeks. Bottom: The relationship between age and PR-VEP P1 peak latencies. Squares represent preterm, whereas circles indicate full-term infants. The solid curves represent the common logistic fit to the merged preterm and full-term data set. For both DRDC-VEP phases and P1 peak latencies, common logistic fit could be established when the adjusted scale was used. Dashed line arrows project the developmental window centers (large black dot on the logistic function) to the age scale. The framed values above the arrows show the exact values for the developmental window centers in weeks, which are determined by the logistic fit parameter ''c.'' Fitting the logistic curve in the very young age range where binocularity does not exist has theoretical (mathematical) meaning only; however, it clearly demonstrates the irrelevance of the calculated developmental window center when postnatal ages are used (top left).**

The counterclockwise phase shift of DRDC-VEPs (Fig. 4) and the rapid decrease of PR-VEP P1 peak latencies observed in this study occur at nearly identical postconceptual (i.e., adjusted) ages. This phase change is most probably due to the same developmental factors that result in the decrease of P1 peak latency. Both the phase shift and P1 peak latency are likely footprints of myelination and gradually faster retino-cortical (may be intracortical) processing of binocular information in the visual system. Both developmental indicators PR-VEP P1 peak latency and DRDC-VEP phase show a developmental pattern that suggests an intrinsic, experience-independent developmental process in the background. The most important underlying mechanism is presumably the intense myelination of the optic nerves and tracts in the first 16 to 18 postnatal weeks. The phase change is robust in premature infants because of the earlier onset of binocularity. In most full-term infants, the phase shift cannot be detected because the binocularity appears when the early phase of the rapid myelination period is over.

Processing speeds can vary between processing channels of the visual system in the mature organism. In another study (Kóbor et al., 2017), we examined colour opponent neurones of domestic cats. Cats are dichromatic animals possessing one cone type in the short wavelength sensitive range (S) and one cone type in the medium-long (ML) wavelength range. We recently described a colour opponent blue-ON cell population from the deep (C-) layers of the lateral geniculate nucleus of cats (Buzás et al., 2013). We proposed that blue-ON cells of the cat exemplify a primordial chromatic pathway thought to be common in ancestral mammals. Here, we showed that blue-ON cells are tuned to much lower frequencies than achromatic cells which do not receive S-cone inputs (Fig. 5). We also demonstrate that within the receptive field of blue-ON cells, the S- and ML-cone inputs are in virtually perfect temporal balance (Fig.6).

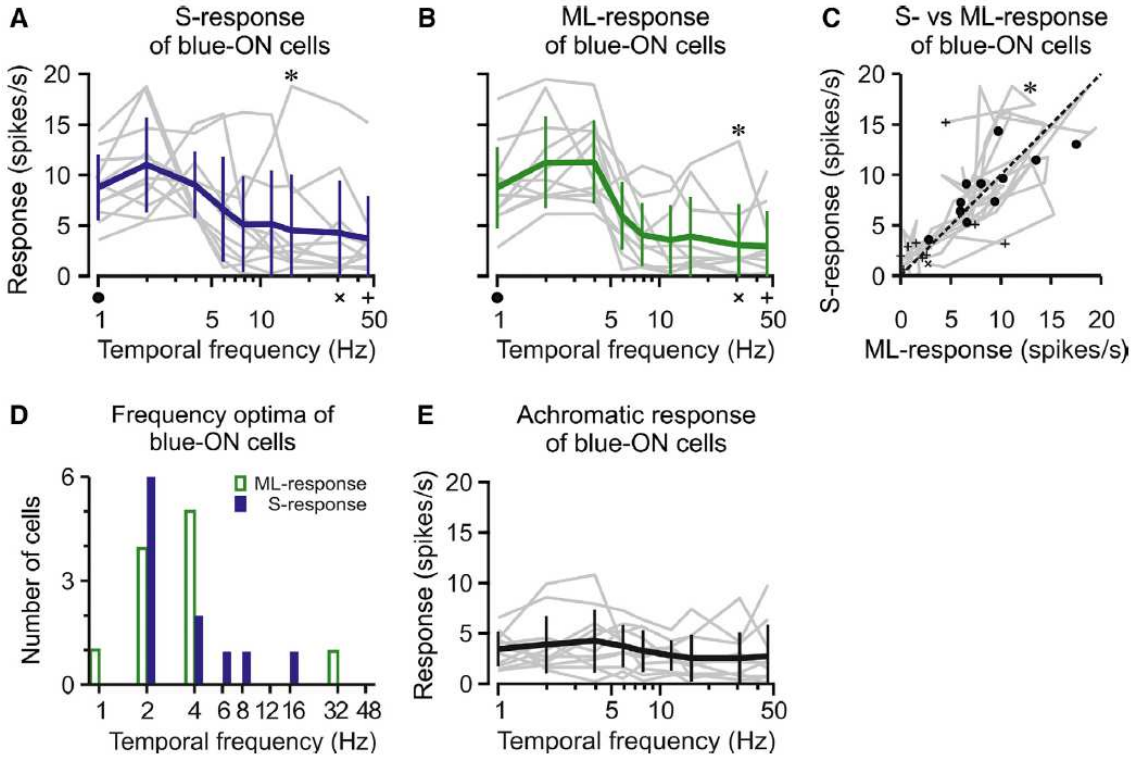

Figure 5. **Temporal frequency tuning of blue-ON cells to cone isolating and achromatic stimulation. Thin grey lines, individual responses; thick lines, average ± SD of tuning curves in A, B and E. (A, B) Blue-ON cells showed low-pass temporal frequency (TF) tuning for both S-cone (A) and ML-cone (B) isolating stimuli. (C) Tuning curves from A and B plotted against each other in order to show**

the correlation of S-cone and ML-cone responses across the entire range of temporal frequencies. Correlation coefficient r = 0.8 ($P < 10^{-6}$). Markers at 1 Hz (●), 32 Hz (9) and 48 Hz (+) indicate the orientation of response trajectories; broken line shows unity. Asterisk indicates tuning curve of one cell with exceptionally high temporal frequency optimum. (D) Distribution of preferred temporal frequencies of blue-ON cells to cone-isolating stimulation. Average preferred frequency for S-cones (filled bars) 3.31 ± 8.85 Hz (geometric mean ± SD) and for ML-cones (open bars) 3.44 ± 4.30 Hz. (E) TF tuning of blue-ON cells for achromatic stimulation. Weak achromatic responses indicate that S-cone and ML-cone inputs have equal functional weight and similar TF tuning.

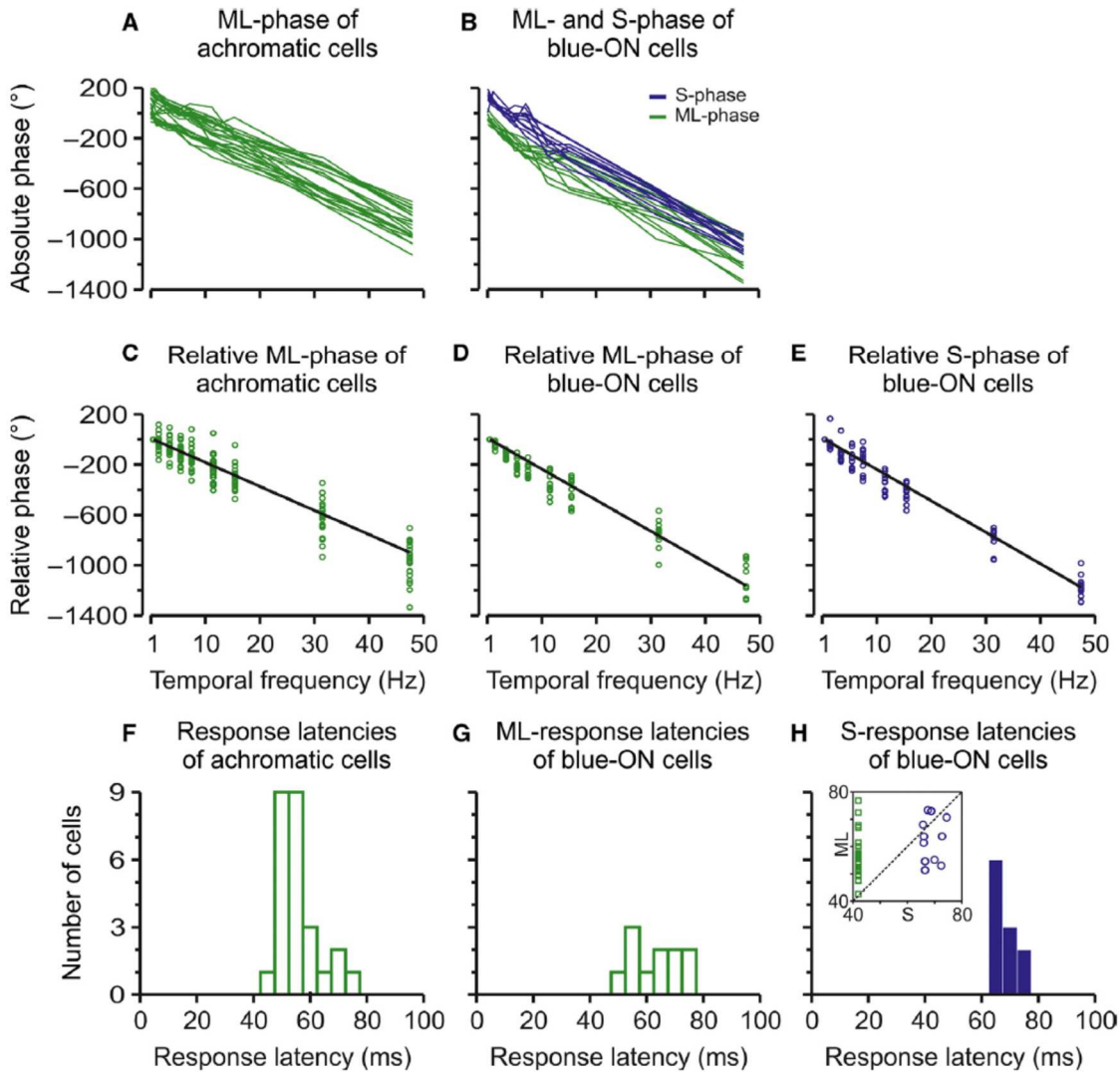

Figure 6. **Visual latencies determined from the phase shift of responses with increasing temporal frequency. (A–B) Raw response phases plotted on a linear scale. (A) Achromatic cells, ML-cone isolating modulation. Each line corresponds to one cell. Note that ON (n = 17) and OFF (n = 9) cells appear as two populations of lines separated by ~180°. (B) Blue-ON cells. S-isolating and ML-isolating responses of each cell are shown by the line types indicated in the legend, respectively. (C–E) Response phases shown relative to the lowest TF tested (1 Hz). The data points of all cells (circles) are fitted with a single regression line. The slope of the line is proportional to visual latency. ML-isolating responses of achromatic cells (C) and ML- (D) and S-cone (E) isolating responses of blue-ON cells are shown. (F–H) Distribution of visual latencies calculated from the**

individual phase shifts shown in C–E, respectively. Mean response latencies for achromatic cells (F) and ML- (G) and S-responses (H) of blue-ON cells were 56 ± 8, 63 ± 8 and 69 ± 3 ms, respectively (mean ± SD). Inset in H shows ML- vs. S-cone latencies for blue-ON cells (circles) and ML-cone latencies for achromatic cells (squares). Unity is indicated by broken line.

The present data, taken together with the spatial properties of cat blue-ON cell receptive fields (Buzás et al., 2013), are compatible with results from macaque blue-ON small bistratified cells in showing the S-ON-inputs are in spatial and temporal balance with the ML-OFF-inputs (Crook et al., 2009). In comparative context, these common features suggest that blue-ON receptive fields in cats and monkeys are adapted to detection of chromatic contrast. In ecological context, our results are consistent with proposed association of S-cone mediated signals with detection of illumination sources and shadows, to allow rapid navigation through terrestrial and arboreal environments (Mollon, 2006; Conway, 2014).

Several of the parallel visual processing channels originate in circuits of the retina. In a recently submitted manuscript (Telkes et al., 2018) we report on a morphological study of electrical synapses that are essential part of the scotopic (rod) pathway. Connexin-36 (Cx36) is the major constituent of mammalian retinal gap junctions (GJs) positioned in key signal pathways. Here, we examined the laminar and (for the first time in any species) the large-scale topographical distribution of Cx36 punctate immunolabels in the retina of the cat, a classical model of the mammalian visual system. Calretinin-immunoreactive (CaR-IR) cell populations served to outline the nuclear and plexiform layers and to stain specific neuronal populations. CaR-IR cells included horizontal cells in the outer retina, AII amacrine cells and a mixture of conventional and displaced amacrine cells in the inner retina. Cx36-IR plaques of the outer retina were found among horizontal cell dendrites but they were not associated systematically with each other. Diffuse Cx36 immunoreactivity was found in the cytoplasm of AII amacrine cells but no obvious colocalization of Cx36 plaques were observed with either the perikarya or the long varicose dendrites of the CaR-IR non-AII amacrine cells. Cx36 puncta were seen throughout the entire inner plexiform layer but they showed their highest density in the ON sublamina. The densities of AII amacrine cell bodies and Cx36 plaques in the ON sublamina were strongly correlated across a wide range of eccentricities suggesting their anatomical association (Fig. 7). However, the high number of plaques per AII cell strongly suggests that a considerable fraction of Cx36 gap junctions in the ON sublamina is formed by other cell types than AII amacrine cells drawing attention to extensive but little studied electrically coupled networks.

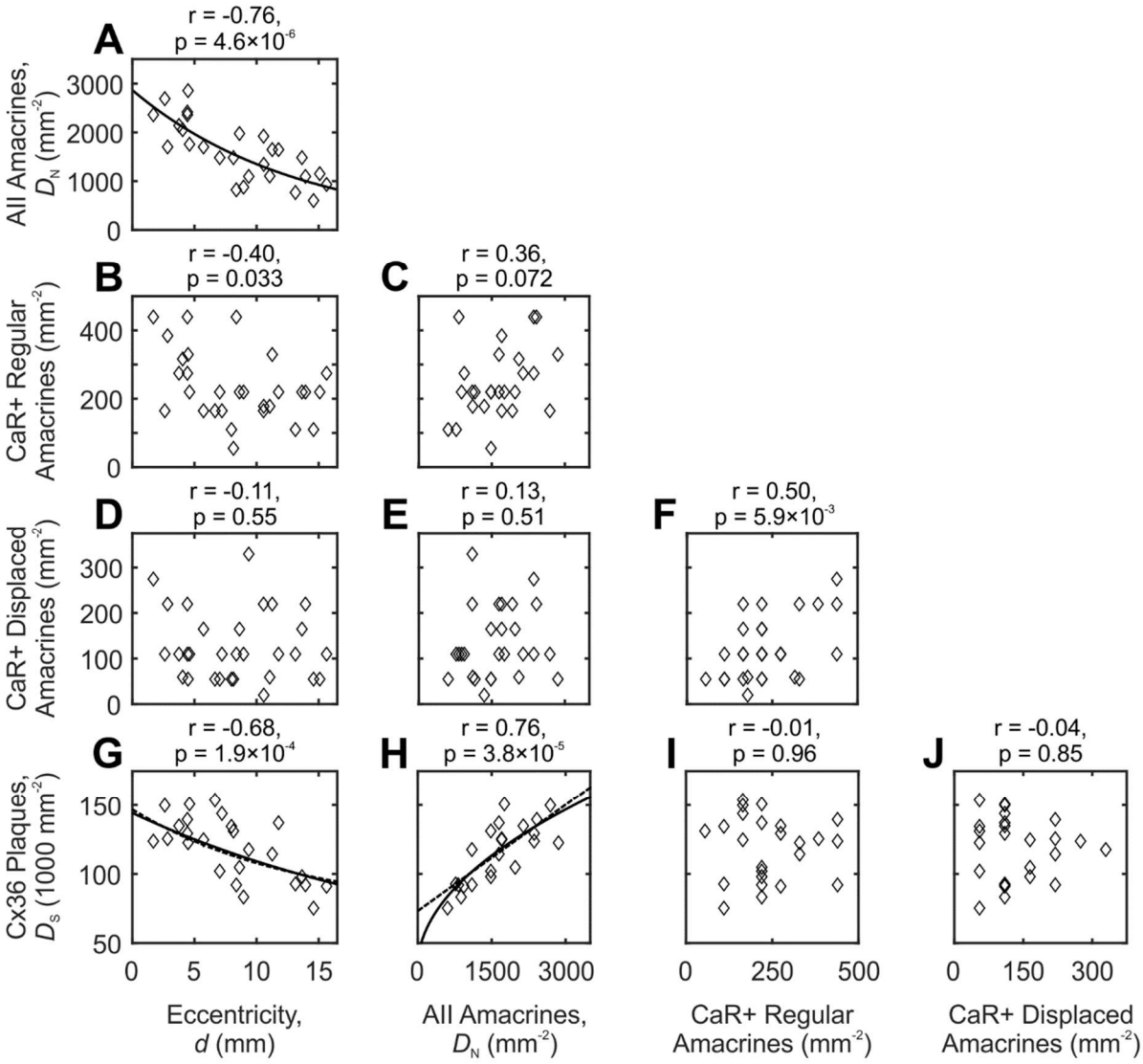

Figure 7. **Pairwise comparisons of the densities of the three Car-IR amacrine cell types, Cx36 puncta and eccentricity. Each data point (diamonds) corresponds to one region of interest. Pearson's correlation coefficients (r) and their significance levels are shown for each pair of measures; p<0.05 was regarded as significant. Alignment of data points in some panels is due to the small (integer) number of strongly labelled amacrine cells in a region of interest. Curves in A, G and H show best fit models of the data. A, exponential decay (R^2=0.60). H, dashed line, linear model (R^2=0.58); solid line, square root model (R^2=0.62). Curves in G were obtained by substituting the respective models in H into the equation of the curve in A to estimate the eccentricity dependence of Cx36 density (R^2=0.49 and R^2=0.50, respectively).**

The processing speed of visual functions can also be studied psychophysically by measuring simple reaction times (RT). Binocular depth perception is an important mechanism to segregate the visual scene for mapping relevant objects in our environment. Convergent evidence from psychophysical and neurophysiological studies have revealed asymmetries between the processing of near (crossed) and far (uncrossed) binocular disparities. The aim of the study described in our paper by Horváth et al. (2018a) was to test if near or far objects are processed faster and with higher contrast sensitivity in the visual system. We therefore measured the relationship between binocular disparity and

simple reaction time (RT) as well as contrast gain based on the contrast-RT function in young healthy adults. RTs were measured to suddenly appearing cyclopean target stimuli, which were checkerboard patterns encoded by depth in dynamic random dot stereograms (DRDS). The DRDS technique allowed us to selectively study the stereoscopic processing system by eliminating all monocular cues. The results showed that disparity and contrast had significant effects on RTs. RTs as a function of disparity followed a U-shaped tuning curve indicating an optimum at around 15 arc min, where RTs were minimal. Surprisingly, the disparity tuning of RT was much less pronounced for far disparities. At the optimal disparity, we measured advantages of about 80 ms and 30 ms for near disparities at low (10%) and high (90%) contrasts, respectively. High contrast always reduced RTs as well as the disparity dependent differences. Furthermore, RT-based contrast gains were higher for near disparities in the range of disparities where RTs were the shortest (Fig. 8). These results show that the sensitivity of the human visual system is biased for near versus far disparities and near stimuli can result in faster motor responses, probably because they bear higher biological relevance.

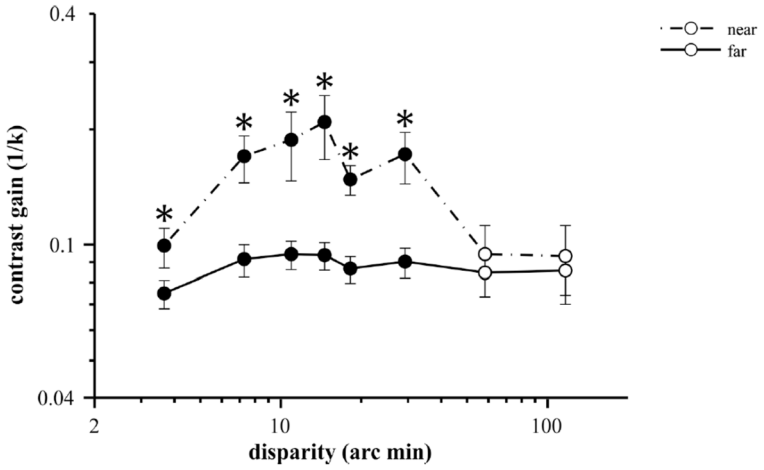

Figure 8. **Representation of the RT-based contrast gain k^{-1} for near and far disparities. Solid line shows the near and the dashed line the far disparities. Asterisks mark disparity values where the contrast gains for near and far stimuli were significantly different (*p<0.05, paired t-test of log transformed data). The data points represent means of 15 participants, error bars show ±SEM.**

The low level binocular correlation mechanisms, also called spatial cross-correlation can be best studied by using random dot correlograms (RDCs). In these stimuli, the degree of correlation between the images/neural inputs of the two eyes can be arbitrarily varied; if their luminance profile is the same, there is a 100% luminance match and the correlation coefficient is 1 (correlated RDC, "C"). A special case of the luminance profile is when all the corresponding dots have the opposite luminance, and every bright dot in one image corresponds to a dark dot in the other image and vice versa, resulting in a 0% luminance match for the two eyes (anticorrelated RDC, "A"). The correlation coefficient is -1 in this case. If the two random dot images are generated independently from each other, their correlation coefficient is 0 (ucorrelated RDC, "U").

Interocular correlation mechanisms have been studied by measuring the time taken to detect changes of correlation states in dynamic random dot arrays (Julesz and Tyler, 1976). In their experiment, Julesz and Tyler presented random dot stimuli that were uncorrelated, anticorrelated or correlated and measured the threshold duration of stimulus presentation needed to recognize a brief change between these correlation states. According to their model, the anticorrelated state invokes the hypothetical "rivalry mechanism" whereas the correlated state invokes the hypothetical "fusion mechanism". Switch from a higher order state (C) to a less ordered state (A or U) will require the

shortest presentation time, a change that stimulates the fusional mechanisms the most. Transitions between U and A states were the most difficult to detect, with A to U state requiring the longest presentation time out of all conditions, which they explained by the long time constant of the "rivalry mechanism". Rivalry is thus slower and less stable, while fusion is stronger and faster neural process. Since responses were modest when both systems were stimulated, in the uncorrelated state, this implies that the two mechanisms inhibit each other. In our previous study (Horváth et al., 2018a) we could detect the variation of simple reaction time (RT) as a function of disparity and contrast. In a manuscript currently in preparation (Horváth et al., 2018b), we are interested to explore whether we could demonstrate the separation of the above mechanisms as simple RT differences for RDC stimuli of different correlation levels and contrasts. We were interested to further investigate the existence of separate, inhibitory mechanisms that might exist for rivalry and fusion, the latter being the dominant and stronger of the two.

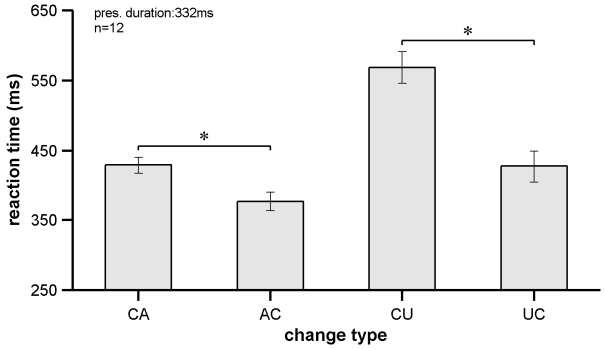

Figure 9. **The effect of the changes direction for mean RTs at 10% contrast. Bars show the mean of the 12 subjects with ±SEM. Significant differences are marked with black asterisks (p≤0.023).**

Reaction times for supra-threshold presentation durations were consistently shorter when the change in correlation was towards the correlated state consistent with the faster response of the putative fusion mechanism (Fig. 9). Our data suggest that binocular correlation is the most persistent and anti-correlation is the least persistent neuronal state in the visual cortex.

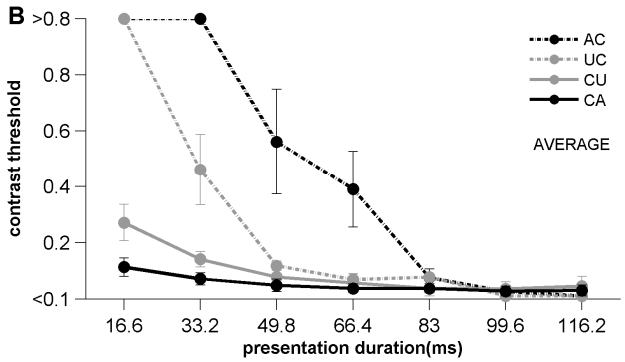

Figure 10. **The effect of presentation duration and contrast for perception of different transitions. Different lines show average contrast thresholds (n = 4 participants) for AC, UC, CU, CA transitions when varying presentation duration determined using adaptive threshold search algorithm.**

Interestingly however, contrast thresholds were higher and the required presentation durations longer for detecting AC or UC transitions (Fig. 10) than for the opposite directions, which appears to contradict the reaction time data. We suggest that although binocular anticorrelation delays the detection of binocular correlation by inhibiting it for about 80 ms, the removal of inhibition results in

a rebound activation accelerating the integration of sensory evidence followed by earlier motor response.

Maturation of binocular vision in humans starts immediately after birth; at around 4-6 months of age, EEG correlates of binocular processing are already present (Jandó et al., 2012). Disparity sensitivity reaches adult-like level by the age of 12 months. Visual cortical connections involved in binocular processing remain, however, plastic until an age of about 7-9 years. Perturbations of the visual experience resulting in incompatible images in the two eyes (e.g. by squinting or optical aberrations) during the critical period influence the development of binocular vision and may lead to suppression of the input from one eye leading to the clinical syndrome of amblyopia. Life-long vision loss on the amblyopic eye can range from two lines on the logMAR scale to complete blindness, which cannot be corrected by lenses. Amblyopia has a prevalence of 3-5% in the population and it is the main reason of monocular vision loss below the age of 70. Although there is no effective therapy for amblyopia after the critical period, it can be prevented and/or treated if risk factors are identified in early childhood. We have found previously that the quality of *stereopsis is a sensitive marker* of visual impairments that disturb normal development of the visual system. Thus, the evaluation of stereoscopic vision in pre-school children promises an effective way of identifying pathological conditions requiring further medical attention.

Stereo vision tests are widely used in the clinical practice for screening amblyopia and amblyogenic conditions. According to literature, none of these tests seems to be suitable to be used alone as a simple and reliable tool. There has been a growing interest in developing new types of stereo vision tests, with sufficient sensitivity to detect amblyopia. This new generation of assessment tools should be computer based, and their reliability must be statistically warranted. Our recently published study (Budai et al., 2018) reports the clinical evaluation of a screening system based on random dot stereograms using a tablet as display. Specifically, a dynamic random dot stereotest with binocularly detectable Snellen-E optotype (DRDSE) was used and compared with the Lang II stereotest.

A total of 141 children (aged 4–14, mean age 8.9) were examined in a field study at the Department of Ophthalmology, Pécs, Hungary. Inclusion criteria consisted of diagnoses of amblyopia, anisometropia, convergent strabismus, and hyperopia. Children with no ophthalmic pathologies were also enrolled as controls. All subjects went through a regular pediatric ophthalmological examination before proceeding to the DRDSE and Lang II tests.

DRDSE and Lang II tests were compared in terms of sensitivity and specificity for different conditions. As shown in Fig. 11, DRDSE had a 100% sensitivity both for amblyopia (n = 11) and convergent strabismus (n = 21), as well as a 75% sensitivity for hyperopia (n = 36). However, the performance of DRDSE was not statistically significant when screening for anisometropia. On the other hand, Lang II proved to have 81.8% sensitivity for amblyopia, 80.9% for strabismus, and only 52.8% for hyperopia. The specificity of DRDSE was 61.2% for amblyopia, 67.3% for strabismus, and 68.6% for hyperopia, respectively. Conversely, Lang II showed about 10% better specificity, 73.8% for amblyopia, 79.2% for strabismus, and 77.9% for hyperopia.

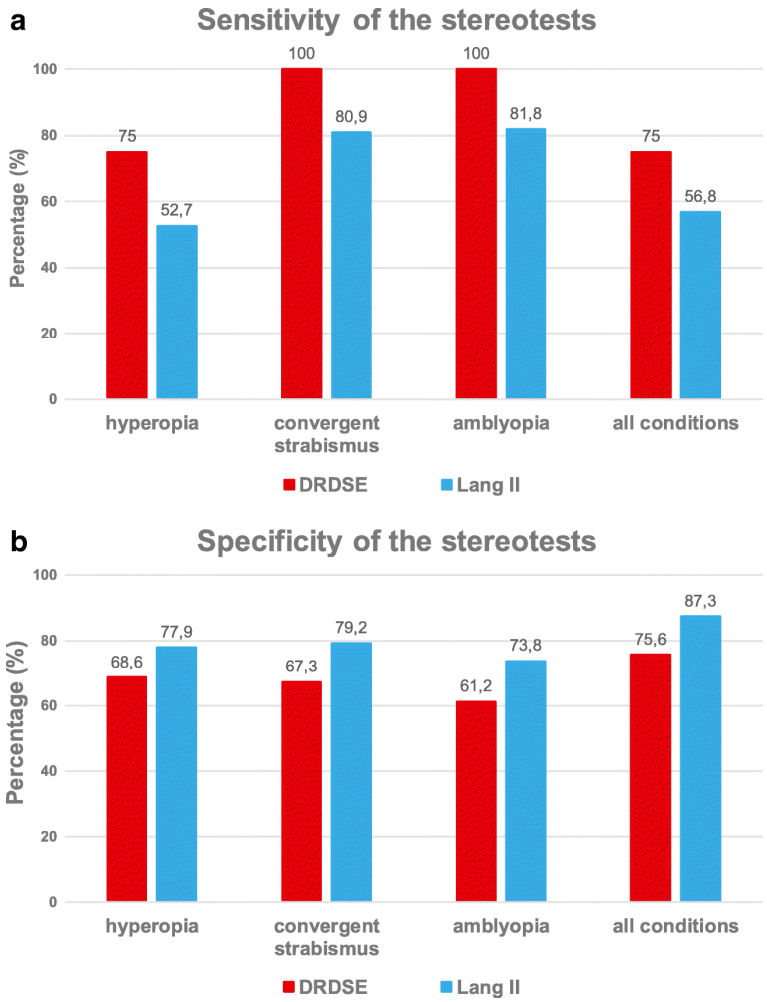

Figure 11. **Bar charts for the comparison of the sensitivity (a) and specificity (b) values of the Lang II test (blue bars) and the DRDSE (red bars). Find exact percent values on the top of each bar.**

The DRDSE test has a better sensitivity for the detection of conditions such as amblyopia or convergent strabismus compared with Lang II, although with slightly lower specificity. If the specificity could be further improved by optimization of the stimulus parameters, while keeping the sensitivity high, DRDSE would be a promising stereo vision test for screening of amblyopia.

REFERENCES

Budai A, Czigler A, Mikó-Baráth E, Nemes V, Horváth G, Pusztai Á, Pinero D, Jandó G (2018) Validation of dynamic random dot stereotests in pediatric vision screening. Graefe's Archive for Clinical and Experimental Ophthalmology 10.1007/s00417-018-4147-x:1-11.

Buzás P, Kóbor P, Petykó Z, Telkes I, Martin PR, Lénárd L (2013) Receptive field properties of color opponent neurons in the cat lateral geniculate nucleus. J Neurosci 33:1451-1461.

Conway BR (2014) Color signals through dorsal and ventral visual pathways. Vis Neurosci 31:197-209.

Crook JD, Davenport CM, Peterson BB, Packer OS, Detwiler PB, Dacey DM (2009) Parallel ON and OFF cone bipolar inputs establish spatially coextensive receptive field structure of blue-yellow ganglion cells in primate retina. J Neurosci 29:8372-8387.

Horváth G, Nemes VA, Radó J, Czigler A, Török B, Buzás P, Jandó G (2018a) Simple reaction times to cyclopean stimuli reveal that the binocular system is tuned to react faster to near than to far objects. PLoS One 13:e0188895.

Horváth G, Nemes V, Radó J, Czigler A, Török B, Kovács I, Buzás P, Jandó G (2018b) Disinhibition can explain faster reaction times to binocularly correlated targets following anticorrelated stimulation. (in preparation).

Jandó G, Mikó-Baráth E, Markó K, Hollódy K, Török B, Kovács I (2012) Early-onset binocularity in preterm infants reveals experience-dependent visual development in humans. Proc Natl Acad Sci U S A 109:11049-11052.

Julesz B (1960) Binocular depth perception of computer-generated patterns. Bell Sys Tech J 39:1125-1162.

Julesz B, Tyler CW (1976) Neurontropy, an entropy-like measure of neural correlation, in binocular fusion and rivalry. Biol Cybern 23:25-32.

Kóbor P, Petykó Z, Telkes I, Martin PR, Buzás P (2017) Temporal properties of colour opponent receptive fields in the cat lateral geniculate nucleus. Eur J Neurosci 45:1368-1378.

Markó K, Mikó-Baráth E, Kiss HJ, Török B, Jandó G (2012) Effects of luminance on dynamic random-dot correlogram evoked visual potentials. Perception 41:648-660.

Mikó-Baráth E, Markó K, Budai A, Török B, Kovács I, Jandó G (2014) Maturation of cyclopean visual evoked potential phase in preterm and full-term infants. Invest Ophthalmol Vis Sci 55:2574-2583.

Mollon J (2006) Monge: The Verriest lecture, Lyon, July 2005. Vis Neurosci 23:297-309.

Radó J, Sári Z, Jandó G, Buzás P (2018) Numerical and analytical solutions for the calibration of computer dislpays to present cyclopean random dot visual stimuli with controlled contrast and luminance. (in preparation).

Telkes I, Kóbor P, Orbán J, Völgyi B, Buzás P (2018) Connexin-36 Distribution and Layer-specific Topography in the Cat Retina. (submitted for publication).

Victor JD, Mast J (1991) A new statistic for steady-state evoked potentials. Electroencephalogr Clin Neurophysiol 78:378-388.